20.8% slot-die coated MAPbI3 perovskite solar cells by optimal DMSO-content and age of 2-ME based precursor inks

Jinzhao Li
Helmholtz Zentrum Berlin
Janardan Dagar
Helmholtz Zentrum Berlin
Oleksandra Shargaieva
Helmholtz Zentrum Berlin
Daniel Többens
Helmholtz-Zentrum Berlin
Rahim Munir
University of Calgary
Eva Unger (eva.unger@helmholtz-berlin.de)
Helmholtz Zentrum Berlin https://orcid.org/0000-0002-3343-867X

Article

Keywords: Solution-processed Solar Cell Devices, Film Formation Process, in-situ X-ray Diffraction, Crystalline Intermediate Phase

Posted Date: October 20th, 2020

DOI: https://doi.org/10.21203/rs.3.rs-93765/v1

Abstract

Solar cells incorporating metal-halide perovskite (MHP) semiconductors are continuing to break efficiency records for solution-processed solar cell devices. Scaling MHP-based devices to larger area prototypes is a crucial step towards commercialization. This requires the development and optimization of scalable process technology for these devices. Here, we demonstrate a maximum power conversion efficiency (PCE) of 20.83% for slot-die coated gas-quenched small-area methylammonium lead iodide ($MAPbI_3$) devices. Our ink is based on 2-methoxy-ethanol (2-ME) with the strongly coordinating solvent dimethyl-sulfoxide (DMSO) added in small amounts. We found that the amount of DMSO, as well as the age of the precursor solutions, are determining factors in achieving highly efficient and reproducible devices. Through in-depth insight into the film formation process as a function of DMSO content from in-situ X-ray diffraction experiments, we found that just the right amount of DMSO favorably affects thin film growth. Adding 11.77 mol% of DMSO prevents the formation of a crystalline intermediate phase related to $MAPbI_3$ and 2-ME ($MAPbI_3$ -2-ME), reported here for the first time, and inducing the formation of some $(DMSO)_2MA_2Pb_3I_8$ intermediate phase. These results demonstrate that ink composition and process control are critical to enable reproducible large-scale manufacturing of MHP-based devices for commercial applications.

Introduction

Metal-halide perovskite (MHP) semiconductors are of interest for various opto-electronic devices: photovoltaics (PV)1–4, light-emitting diodes (LED)5, lasers6, and photodetectors7. With 25% power conversion efficiency (PCE),8 MHP solar cell devices are the best solution-processed solar cell devices to date.2 Having reached performance on par with other thin-film devices in laboratory-scale test devices, scaling MHP-based solar cells to a larger area is one of the technologically most important steps.
A variety of scalable fabrication techniques such as blade coating9, vapor-assisted deposition10, inkjet printing11 and slot-die coating (SDC)12 have been successfully utilized for the deposition of MHP materials. Notably, SDC is considered as one of the promising deposition techniques in the fabrication of functional coating and solution-processed optoelectronics electronics fields due to its advantages of making uniform and compact thin films on both rigid and soft substrates13. When coating crystalline (or crystallizing) materials such as MHP, the quality of the thin film is determined by the coating process. Fabricating high-quality thin films requires exact control over the process window and removal of solvents at a defined period of time to induce oversaturation and crystallization in a controlled manner. Solvent removal can be facilitated by thermal annealing14, vacuum12, gas quenching15 or the deposition of an anti-solvent, which for larger area samples is often accomplished by dipping into a bath.16
Currently, the PCE obtained for slot-die coated devices is lower than record device PCEs achieved by spin-coating17. This is due to the fact that there has been considerably less optimization work on SDC for MHP deposition and record-performance spin-coated devices rely on rapid solvent removal and induction

of crystallization by deposition of an anti-solvent. One of the most important aspects to optimize slot-die coating for MHP deposition is to develop reproducible coating processes where the MHP crystallization is selectively induced during the coating process. Process optimization and design of stable precursor inks that enable the deposition of high quality MHP layers that yield higher PCE in solar cell devices.
In this work, we successfully slot-die coated methylammonium lead iodide (MAPbI3) thin films from a low boiling point and highly soluble 2-methoxy-ethanol (2-ME) ink as previously introduced by Hendriks et al. in spin-coating.18 Deng et al. adopted this ink to realize blade-coated PSCs9 introducing the strongly coordinating solvent dimethyl sulfoxide (DMSO) to improve the quality of coated perovskite thin films. We here demonstrate, that record-performance slot-die coated PSCs can be manufactured following this procedure and provide a detailed investigation on how the exact amount of DMSO and age of the precursor ink affects thin-film morphology as well as device performance. Record performance device were achieved for 11.77 mol% of DMSO in the precursor solution. Using in-situ grazing incidence X-ray scattering experiments, we can prove that adding a small amount of DMSO leads to the suppression of a crystalline intermediate phase related to MAPbI3 and 2-ME (here referred to as MAPbI3-2-ME) in favor of the formation of MAPbI3 seed crystals and a limited amount of the (DMSO)2MA2Pb3I8 intermediate phase. A larger amount of DMSO and with proceeding age of the precursor solution, the precipitation of the crystalline (DMSO)2MA2Pb3I8 solvate phase19 becomes detrimental to the perovskite thin film morphology. We highlight that both the exact amount of DMSO as well as the age of the precursor solution critically affect the coating results and device performance. This is critical insight to enable the development of stable and reproducible coating procedures for large scale manufacturing of perovskite solar cell devices. At an optimal content of about 12 mol% DMSO in the 2-ME ink, we demonstrated champion MHP device with efficiency of 20.83%, which is among the highest value reported in slot-die coated PSCs.

Results And Discussion

As MHP tends to crystallize during deposition, the removal of solvents at a defined point in time determines the thin film quality. This provides some but limited control over the process window and the exact composition of the ink has a significant influence on the quality of the MHP semiconductor. In the process discussed here, this was achieved by N2 gas quenching through an air knife at around 20 cm distance relative to the slot-die as illustrated in Figure 1. 2-methoxy ethanol (2-ME) is a low boiling point (Tb = 124°C) and high vapor pressure (~ 0.8 kPa at 20 ºC) solvent with maximum solubility around 2.4 M of MAPbI3.18 During coating, the ink is dispensed from the slot-die head onto the substrates, as sketched in Figure 1.a. Therein, MHP films were discontinuous and porous coated from 2-ME ink. We attribute this to the rapid MHP crystallization from inks without DMSO additives when 2-ME spontaneously evaporates during coating and air knife gas quenching.

Addition of small amounts of the strongly coordinating solvent DMSO led to dramatically changes of the ink properties and coating process. In Figure 1 b, the morphology of samples coated from inks with various amounts of DMSO, from 11.77 mol% to 58.88 mol%, are compared. Samples coated from a 2-ME

ink, exhibit a disrupted morphology with pinholes density around 7% (Supplementary Figure 1). The addition of 11.77 mol% DMSO into 1M 2-ME ink leads to a denser thin-film without pinholes while with higher DMSO contents the crystallite size becomes smaller as shown in Figure 1 c. Moreover, inks with added DMSO exhibited a yellow precipitate increasing with time and DMSO content when stored at room temperature as shown in Figure 1 d. The 2-ME precursor ink without DMSO and the 2-ME based ink comprising 11.77 mol% of added DMSO do not exhibit this precipitate. This suggests a chemical interaction between the DMSO and perovskite precursors. As previously reported9, without the addition of MAI, PbI2 has a limited solubility in 2-ME. As a strong coordinating solvent, DMSO can be expected to increase the solubility of the precursor salts in 2-ME. However, DMSO is known to interact strongly with MAPbI3 in the solid-state phase forming the crystalline intermediate phase ((DMSO)2MA2Pb3I8)20. As this DMSO intermediate phase has limited solubility in 2-ME, a higher content of DMSO in 2-ME solution leads to precipitation. The precipitate was identified by XRD as (DMSO)2MA2Pb3I8.20 After annealing the precipitate, the color converted to black and intensity of the diffraction peaks associated with the perovskite phase appeared (Supplementary Figure 2).

In-situ grazing-incidence wide-angle X-ray scattering (GIWAXS) was utilized to investigate the drying kinetics as a function of DMSO content with respect to the 2-ME ink (Figure 2). The sample deposited from 2-ME ink initially (start to 0.5 minutes, see Supplementary Figure 3) exhibits broad features at low diffraction angles indicating the presence of a crystalline sol-gel intermediate state. As visible in the 2D representation of the evolution of diffraction patterns during drying in Figure 2a, until about 1 minute into the process diffraction peaks at 2theta angles of 5.92° and 11.86° are visible. We attribute these to a crystalline solvate intermediate phase of MAPbI3 with 2-ME. Upon drying, an intermediate peak at 2theta angles of 8.15°, appearing after 1.4 minutes and disappearing after 3 minutes, indicates the formation of another intermediate phase. This phase may be comparable to the (MA)8(Sol)xPb18I44 intermediate phase reported by Lei et al22. Fast evaporation of 2-ME results in the rapid transformation of this intermediate phase into MHP phase after only 1 minute at 25 °C. This can be observed as an evolution of the diffraction peak at 14.08° that correlates with the (110/002) peaks of the room temperature tetragonal MAPbI3 phase23. It can be noted that the MHP peak intensity is relatively high, indicating rapid crystallization of the MHP as 2-ME solvent starts evaporating.
When adding 11.77 mol% of DMSO into 1 M 2-ME ink as shown in Figure 2b, d, a diffraction peak at 5.92° suggest the initial co-existence of the intermediate phases of MAPbI3-2-ME and the DMSO solvate phase with known diffraction peaks at 6.55°, 7.2°, 9.17° attributed to (DMSO)2MA2Pb3I8 during the first 0.5 minute of the process20. There is no peak at 8.15° visible in this case suggesting that the formation of this second intermediate phase is suppressed. Instead, a diffraction pattern consistent with the formation of crystalline MAPbI3 is visible from the start as shown in Figure 2 c, d. We interpret these findings that the DMSO additive avoids the formation of the 2-ME solvate phase and triggers the formation of MAPbI3 as well as DMSO solvate phase. These results indicate the formation of MAPbI3 seed crystals upon addition of DMSO, which favorably affects thin film formation. We hypothesize, that the much higher binding constant of DMSO to lead-halide complexes in solution disrupts the formation of the 2-ME and

other solvate intermediate phases to promote the formation of crystalline MAPbI3. Simultaneously, (DMSO)2MA2Pb3I8 is also formed, which, at small concentrations, may prove beneficial to thin film formation as it may increase the processing window. That the formation of the (DMSO)2MA2Pb3I8 intermediate phase is detrimental at higher concentration becomes apparent when increasing to the amount of added DMSO to over 11.77 mol% (Figure 2d, Supplementary Figure 4), which leads to a disappearance of any MAPbI3-2-ME intermediate but also the MAPbI3 phase in favor of (DMSO)2MA2Pb3I8. The formation of the DMSO solvate phase occurs already in solution apparent by the formation of the yellowish precipitate in precursor solutions shown in Figure 1.c. In this case, MAPbI3 has to and increasing extent be formed by decomposition of the DMSO intermediate phase. This negatively affects the thin-film morphology as shown in the SEM cross section images in Figure 1.b. To compare ink properties, ex-situ GIWAXS was employed to detect crystallinity and orientation of MHP semiconductors. We did not observe a change in orientation, indicating the crystal growth orientation wasn't affected by the addition of DMSO (Supplementary Figure 5). However, the 2ME-DMSO samples exhibit an increased intensity of the diffraction peaks associated with the perovskite crystal phase. We conclude that the addition of DMSO improves the crystallinity of the thin-film sample (Supplementary Figure 6).

To study the stability of precursor inks. A series of devices were prepared from precursor inks with various amounts of DMSO (11.77 mol% - 58.88 mol%) and time elapsed since preparation of the ink 1, 5, 10, 30 and 60 min in comparison to the reference ink. Figure 3.a show the device configuration is glass | ITO (150 nm) | 2PACz | MAPbI3 (~ 800 nm) | C60 (23 nm) | BCP (8 nm) | Cu (100 nm) where 2PACz is a self-assembled monolayer (SAM) of (([2-(9H-carbazol-9-yl)ethyl]phosphonic acid)). The results shown in Figure 3b clearly illustrate the dependency of the PCE obtained in solar cells on the DMSO content and age of the precursor ink. The devices made from the 2-ME reference ink exhibit fairly low and irreproducible performance metrics. For an increasing content of DMSO as an additive in 2-ME precursor inks, the average performance and reproducibility initially increases for intermediate DMSO concentrations of about 12 mol% and 24 mol% but then clearly decreases for higher DMSO content and also with increasing ink age. This is consistent with the observed increase in the formation of a precipitate shown in Figure 1c and UV-Vis measurements on precursor inks as shown in Supplementary Figure 7. The formation of this precipitate inside the narrow tubing and ink reservoir of the slot-die coater will dramatically influence the pump rate and solution feed during the coating process. This leads to random and unrepeatable deposition conditions along with the likely deposition of the (DMSO)2(MA)2Pb3I8 precipitate negatively affecting thin film morphology. To investigate the influence of precipitation on the film nucleation, 23.56 mol% 2ME-DMSO ink was centrifuged at 6,000 rpm for 45 min with this ink without centrifuged were compared, which resulted in similar devices performance (Supplementary Figure 8) and indicates that the precipitate affect the coating process negatively. Optimal contents of DMSO is crucial to stabilize MHP inks. The 11.77 mol% DMSO ink exhibits better long-term stability than the others investigated herein. Even after storing this ink for 18 days, solar cells with a performance of 19.50% were manufactured as shown in Supplementary Figure 9. After storage for 18 days, the 23.56 mol% DMSO content ink exhibited precipitation and could not be used to produce

good quality coatings at all. Figure 3.c show the solar cells prepared from the 11.77 mol% and 23.56 mol% 2-ME-DMSO precursor solutions yielded a maximum PCE of 20.83%, 20.25% compared to 15.42% for the pure 2-ME reference devices. These PCEs are among the highest values reported for slot-die coated PSCs (Supplementary Figure Table 1). The steady-state results of corresponding devices, showing PCE of 20.55%, 19.59% and 14.89% upon 180 seconds maximum power point (MPP) tracking as shown in Figure 3.d.

Table 1. summary of photovoltaic parameters obtained from corresponding *J–V* curves.

	2-ME		11.77 mol% 2-ME-DMSO		23.56 mol% 2-ME-DMSO	
	Reverse	Forward	Reverse	Forward	Reverse	Forward
J_{sc} (mA/cm^2)	19.778	19.565	23.673	23.633	23.686	23.645
V_{oc} (V)	1.085	1.082	1.138	1.132	1.119	1.111
Fill factor (%)	71.870	66.860	77.322	76.426	76.415	75.343
PCE (%)	15.424	14.155	20.831	20.459	20.256	19.793
PCE_{mpp}(%)	14.89		20.55		19.59	

The stability assessment of the champion devices was performed via MPP tracking under continuous 1 sun illumination for 11 hours. We observed a stabilized device efficiency of 19.16% before tracking and 19.24% after tracking for this particular device suggesting a negligible loss in efficiency as shown in Supplementary Figure 10. We compared the device performance with and without shadow mask and found around 3% discrepancy in the JSC (Supplementary Figure 11, Supplementary Table 2). Comparing the integrated EQE spectra with respect to AM1.5 results in JSC values comparable to the ones determined by J-V measurements (Supplementary Figure 12) with a discrepancy < 4%. Additionally, the bandgaps are around 1.58 – 1.59 eV determining by the peak position of the derivative of the EQE spectrum. The 2-ME-DMSO devices exhibit lower leakage current (J0) in the dark J-V curves compared to the 2-ME device as a result of the superior MHP layer morphology as discussion in the Supplementary Information (Figure S13). The 11.77 mol% 2-ME-DMSO device shows an improved rectification leading to the better performance in the reverse bias condition of the MHP based solar cell24.
Transient analysis during maximum power point tracking (TrAMPPT) was used to investigate the devices hysteresis behavior upon voltage perturbation, further discussed in the Supporting Information 25,26. The comparison of the transient with respect to the steady-state current density, $\frac{\Delta J(t)}{Jss}$ and the hysteresis index (HI) as function of delay time derived from J-V measurements (Supplementary Figure 16) of the 2-ME, 11.77 mol% and 23.56 mol% 2-ME-DMSO devices as shown in Figure 3 e. The devices prepared from precursor solutions with DMSO exhibit a dramatically reduced $\frac{\Delta J(t)}{Jss}$ HI for fast scan rates corresponding

to short delay times. The device fabricated from the pure 2-ME precursor ink exhibits a more pronounced amplitude of the transient current response for fast J-V scan rates compared to the devices fabricated from inks containing small amounts of DMSO where this transient current response is fairly suppressed. This directly corresponds to a reduction of the hysteresis for fast scan-rates that suggest capacitive effects or sluggish charge carrier extraction for devices with inferior perovskite thin film morphology. We conclude that the smaller grain size and higher degree of disorder and pinholes of samples prepared without the DMSO additive in the precursor solutions gives rise to more sluggish charge carrier extraction and hence larger amplitudes in the transient current response upon voltage perturbation.

Conclusions

In conclusion, we were able to achieve highly PCEs of slot-die coated perovskite solar cells reproducibly when just the right amount of DMSO is added to 2-ME based precursor solutions. For an amount of about 12 mol% DMSO, a stable ink with a beneficial coating process window can be obtained enabling the deposition of high-quality MHP thin-films and high-performance solar cell devices. From in-situ X-ray diffraction experiments we have discovered the existence of a solvent intermediate phase involving 2-ME and MAPbI3 which rapidly converts to MAPbI3 upon drying. The addition of DMSO leads to the suppression of this intermediate phase and formation of MAPbI3 seed crystals as well as some (DMSO)2MA2Pb3I8 intermediate phase, which favorably affects the formation process of MAPbI3 during slot-die coating. This leads to MAPbI3 thin-films with improved morphology. For a higher DMSO content the suppression of MAPbI3 formation in favor of (DMSO)2MA2Pb3I8 reduces thin-film layer quality and reproducibility as the crystalline DMSO-solvate phase precipitate negative affects thin-film formation and morphology. From inks with optimal DMSO content, slot-die coated p-i-n solar cell device with efficiency of 20.83% (stabilized output at 20.55%) were demonstrated. This work provides important insight into the interplay of strongly and weakly coordinating solvent as well as crystalline intermediate phases in the formation of MHP thin-films. Control over exact processing conditions and formation pathways is key to develop stable and reproducible scalable coating procedures, which is crucial for the commercial fabrication of MHP semiconductor devices.

Methods

Materials:

Lead (II) Iodide (99.99%, trace metals basis), SAM (([2-(9H-carbazol-9-yl)ethyl]phosphonic acid), 2PACz) were purchased from Tokyo Chemical Industry (TCI). Methylammonium iodide (MAI), was purchased from Dynamo. Bathocuproine (BCP) was purchased from Ossila. Ethanol (anhydrous) was purchased from VWR Chemicals and Copper Shots was purchased from Alfa Aesar. Other chemicals were purchased from Sigma-Aldrich. All the chemicals were used as received without purification.

MHP semiconductors inks preparation

MAI and PbI_2 were mixed in a vial and dissolved with 2-methoxyethanol (2-ME) as a 2-ME ink (1M) and stirring overnight at room temperature. DMSO (around 11.77 mol%, 23.56 mol%, 35.33 mol%, 47.10 mol%, 58.88 mol% DMSO) was put into 2-ME ink before coating.

SAM powders were dissolved in anhydrous Ethanol at a concentration of 0.5mg/ml and put into an ultrasonic bath for 15 min (~ 45 °C) before using[24].

Slot die coating MHP semiconductors and devices fabrication.

The configuration of P-I-N devices

ITO (150nm)/SAM (2PACz)/$MAPbI_3$ (~800 nm)/C_{60} (23 nm)/BCP (8 nm)/Cu (100 nm)

ITO cleaning

The cleaning procedure of patterned Indium tin oxide (ITO, 15 Ω sq-1, 150 nm) are the same with before[26]. In brief, ITO glasses were cleaned by Mucasol solution in deionized water (DI water), DI water, acetone and isopropanol at around 40 °C for 15 minutes each.

SAM preparation

Before spin-coating SAM, the ITO glasses were pre-clean with 15 minutes UV-ozone treatment. Then SAM layer was spin coated at the speed of 3,000 r.p.m for 30 s, (ramping: 1,000/s) and then annealed at 100 °C for 10 min.

SDC MHP semiconductors and devices making

The slot die coater (FOM technologies) which is composed of an ink reservoir, pump systems, slot-die head, and a temperature-controlled bottom plate (vacuum chuck) mounted on a conveyor belt system. An air knife for N_2 gas quenching can be optionally mounted in the system. In brief, when coating begins, the pump systems precisely control how much ink (pump rate) flows through a tube into the slot die head to substrates, and the conveyor system determines the coating speed and direction.

MHP semiconductors inks were pipetted into a syringe connecting to a tube, which is controlled by pump (pump rate fix how much ink is pouring down out of the tube into die head per second). Coating speed is 20 cm/min, pump rate is 50 µl/min, gap is around 0.2-0.3 mm, air knife pressure is approximately 20 psi at room temperature. The MHP semiconductors were annealed at 100 °C for 20 minutes.

After cooling down to room temperature, the substrates were transferred to the evaporation system (MBRAUN ProVap 3G). The BCP (8 nm), C_{60} (23 nm) and copper (100 nm) layers were subsequently deposition by thermal evaporate method. The evaporate rate of BCP is 0.1 Å/s, C_{60} is 0.05 Å/s to 0.1 Å/s, and the rate of copper is 0.1 Å/s to 1 Å/s at base pressure of 1×10^{-6} mbar. For the champion devices, a

100 nm NaF (Sodium Fluoride) layer was deposited upon the glass side at base pressure of 1×10^{-6} mbar, with rate of 0.1 - 1 Å/s

Characterization

J-V

A LabView programmed Keithley 2400 SMU was used to record current–voltage (*J– V*) measurements parameters under AM 1.5G 100 mW/cm^2 (Oriel LCS-100 class ABB solar simulator) in a N_2-filled glovebox, calibrated with silicon reference cell (Fraunhofer ISE). The active area of all devices reported in this work is 0.16 cm^2 defined by the overlap area of patterned ITO and masked copper electrode. A 0.09 cm^2 mask determined by microscope imaging was used to define the active area precisely. The measurement was carried on at room temperature in a N2-filled glovebox without any preconditioning. The scan directions are 1.2 V to −0.02 V (reverse) or −0.02 V to 1.2 V (forward), with 20ms delay time, 40ms integration time and 20mV voltage step. In the *TrAMPPT* measurement, the *J-V* curves of corresponding devices were measured just after the *TrAMPPT* test, with integration time of 0.2 ms, 0.2 ms, 1 ms, 10 ms, 20 ms, 30 ms and settling time of 0.1 ms, 1ms, 10ms, 100ms, 1,000ms, 3,000ms.

EQE

The external quantum efficiency (EQE) measuremnts (from 300 to 850 nm) were performed using Oriel Instruments QEPVSI-b system with a Xenon arc lamp (Newport 300 W, 66902) chopped at 35.5 Hz and a monochromatic instrument (Newport Cornerstone 260)[26].

SEM

The scanning electron measurements (SEM) images (top view and cross-section) were measured by Hitachi S-4100 at 5 kV.

GIWAXS

In-situ grazing incidence wide-angle X-ray scattering (GIWAXS) measurements were conducted at KMC-2 beamline[21] at the synchrotron source BESSY II (Helmholtz-Zentrum Berlin). The photon energy of the source is 8048 eV. Incident angle was fixed at 2 deg. We use the area detector Bruker AXS. The detector was kept on 9 degrees to collect the scattering. An Anton Paar setup was used to control the substrate temperature and the temperature ramp is around 45 °C/min During measurement, the samples were kept under constant nitrogen gas flow (6 liter/hour) connected to the Anton Paar setup.

References

1. Kojima, A., Teshima, K., Shirai, Y. & Miyasaka, T. Organometal halide perovskites as visible-light sensitizers for photovoltaic cells. J. Am. Chem. Soc. 131, 6050–6051 (2009).
2. Zheng, X. et al. Managing grains and interfaces via ligand anchoring enables 22.3%-efficiency inverted

perovskite solar cells. Nat. Energy 5, 131–140 (2020).
3. Lee, Michael M. Teuscher, J. Miyasaka, T. Murakami, T. Snaith, H. J. Efficient Hybrid Solar Cells Based on Meso-Superstructured Organometal Halide Perovskites. Science (80-.). 338, 643–647 (2012).
4. Sahli, F. et al. Fully textured monolithic perovskite/silicon tandem solar cells with 25.2% power conversion efficiency. Nat. Mater. 17, 820–826 (2018).
5. Liu, M. et al. Lattice anchoring stabilizes solution-processed semiconductors. Nature 570, 96–101 (2019).
6. Zhang, N. et al. All-optical control of lead halide perovskite microlasers. Nat. Commun. 10, 1–7 (2019).
7. Miao, J. & Zhang, F. Recent progress on highly sensitive perovskite photodetectors. J. Mater. Chem. C 7, 1741–1791 (2019).
8. Best Research-Cell Efficiency Chart (NREL, accessed 03 August 2020); https://www.nrel.gov/pv/cell-efficiency.html.
9. Deng, Y. et al. Tailoring solvent coordination for high-speed, room-temperature blading of perovskite photovoltaic films. Sci. Adv. 5, eaax7537 (2019).
10. Li, J. et al. Vapor Exchange Deposition of an Air-Stable Lead Iodide Adduct on 19% Efficient 1.8-cm2 Perovskite Solar Cells. ACS Appl. Energy Mater. 2, 2506–2514 (2019).
11. Mathies, F., List-Kratochvil, E. J. W. & Unger, E. L. Advances in Inkjet-Printed Metal-Halide Perovskite Photovoltaic and Optoelectronic Devices. Energy Technol. 81, ente.201900991 (2019).
12. Cai, L. et al. Large area perovskite solar cell module. J. Semicond. 38, 2–5 (2017).
13. Lim, E. & Yao, J. A Review of the Operating Limits in Slot Die Coating Processes. IFAC Proc. Vol. 7, 405–410 (2009).
14. Burkitt, D., Searle, J., A.Worsley, D. & Watson, T. Sequential slot-die deposition of perovskite solar cells using dimethylsulfoxide lead iodide ink. Materials (Basel). 11, (2018).
15. Lee, D. et al. Slot-Die Coated Perovskite Films Using Mixed Lead Precursors for Highly Reproducible and Large-Area Solar Cells. ACS Appl. Mater. Interfaces 10, 16133–16139 (2018).
16. Whitaker, J. et al. Scalable Slot-die Coating of High Performance Perovskite Solar Cells. Sustain. Energy Fuels 2, 2442–2449 (2018).
17. Li, Z. et al. Scalable fabrication of perovskite solar cells. Nat. Rev. Mater. 3, 1–20 (2018).
18. Hendriks, K. H. et al. 2-Methoxyethanol as a new solvent for processing methylammonium lead halide perovskite solar cells. J. Mater. Chem. A 5, 2346–2354 (2017).
19. Lee, J. W., Kim, H. S. & Park, N. G. Lewis Acid-Base Adduct Approach for High Efficiency Perovskite Solar Cells. Acc. Chem. Res. 49, 311–319 (2016).
20. Rong, Y. et al. Solvent engineering towards controlled grain growth in perovskite planar heterojunction solar cells. Nanoscale 7, 10595–10599 (2015).
21. Többens, D. M. & Zander, S. KMC-2: an X-ray beamline with dedicated diffraction and XAS endstations at BESSY II. J. large-scale Res. Facil. JLSRF 2, 1–6 (2016).
22. Lei, L. et al. Morphology and Defect Control of Metal Halide Perovskite Films for High-Performance Optoelectronics. Chem. Mater. (2020) doi:10.1021/acs.chemmater.0c00798.
23. Quarti, C. et al. Structural and optical properties of methylammonium lead iodide across the tetragonal to cubic phase transition: Implications for perovskite solar cells. Energy Environ. Sci. 9, 155–

163 (2016).
24. Talaikis, M. et al. Conformal monolayer contacts with lossless interfaces for perovskite single junction and monolithic tandem solar cells. Energy Environ. Sci. 12, 3356–3369 (2019).
25. Czudek, A. et al. Transient Analysis during Maximum Power Point Tracking (TrAMPPT) to Assess Dynamic Response of Perovskite Solar Cells. arXiv:1906.05028 (2019).
26. Dagar, J. et al. Alkali-Salts as Interface Modifiers in n-i-p Hybrid Perovskite Solar Cells. Sol. RRL 3, 1900088 (2019).

Declarations

Acknowledgements
J.Z.L. acknowledges funding from the Chinese Scholarship Council (CSC, grant No. CSC201908120116). E.U. and her team acknowledge funding from the German Ministry of Education and Research (BMBF) for the Young Investigator Group Hybrid Materials Formation and Scaling (HyPerFORME) within the program “NanoMatFutur” (grant no. 03XP0091) and the SNaPSHoTs project (grant no. 01IO1806). Lab infrastructure in the Helmholtz Innovation Lab was supported by the Helmholtz Energy Materials Foundry (HEMF) and the PEROSEED (ZT-0024) project, as well as the support of the. Allocation of synchrotron radiation beamtime at KMC-2, BESSY II, HZB is gratefully acknowledged.

Author contributions
J.Z.L. conceived the idea under the guidance of E.U. J.Z.L. and J.D. made devices and measured devices performance. J.Z.L. and O.S. measured UV-Vis spectra. J.Z.L. and R.M. carried out the GIWAXS measurements assisted by D.T. J.D., O.S., R.M., and E.U. assisted J.Z.L in the interpretation of experimental results and suggested reference experiments. All authors participated in writing, editing and reviewing the manuscript.

Competing interests
The authors declare no competing interests.

Figures

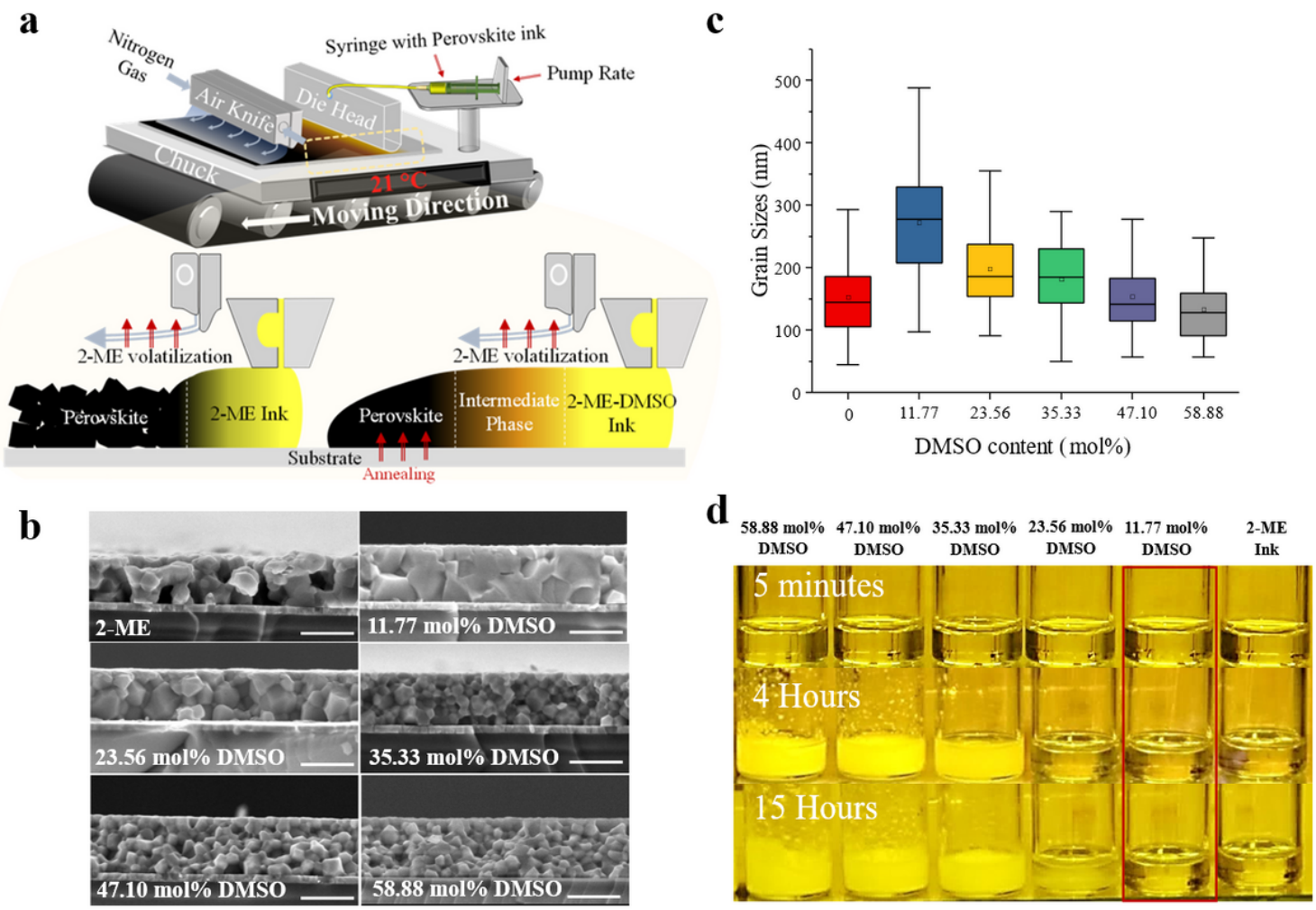

Figure 1

Schematic of slot die coater setup. a, Coating from 2-ME and 2-ME-DMSO inks. b, SEM cross-section images depicting corresponding conditions (scale bar is 800 nm). c, The grain size distribution of corresponding samples determined from SEM top view images in Supplementary Figure 1. d, Images of 2-ME DMSO inks (in duration of 1 to 15 hours) store inside the glovebox (with O2 and H2O level less than 1 ppm).

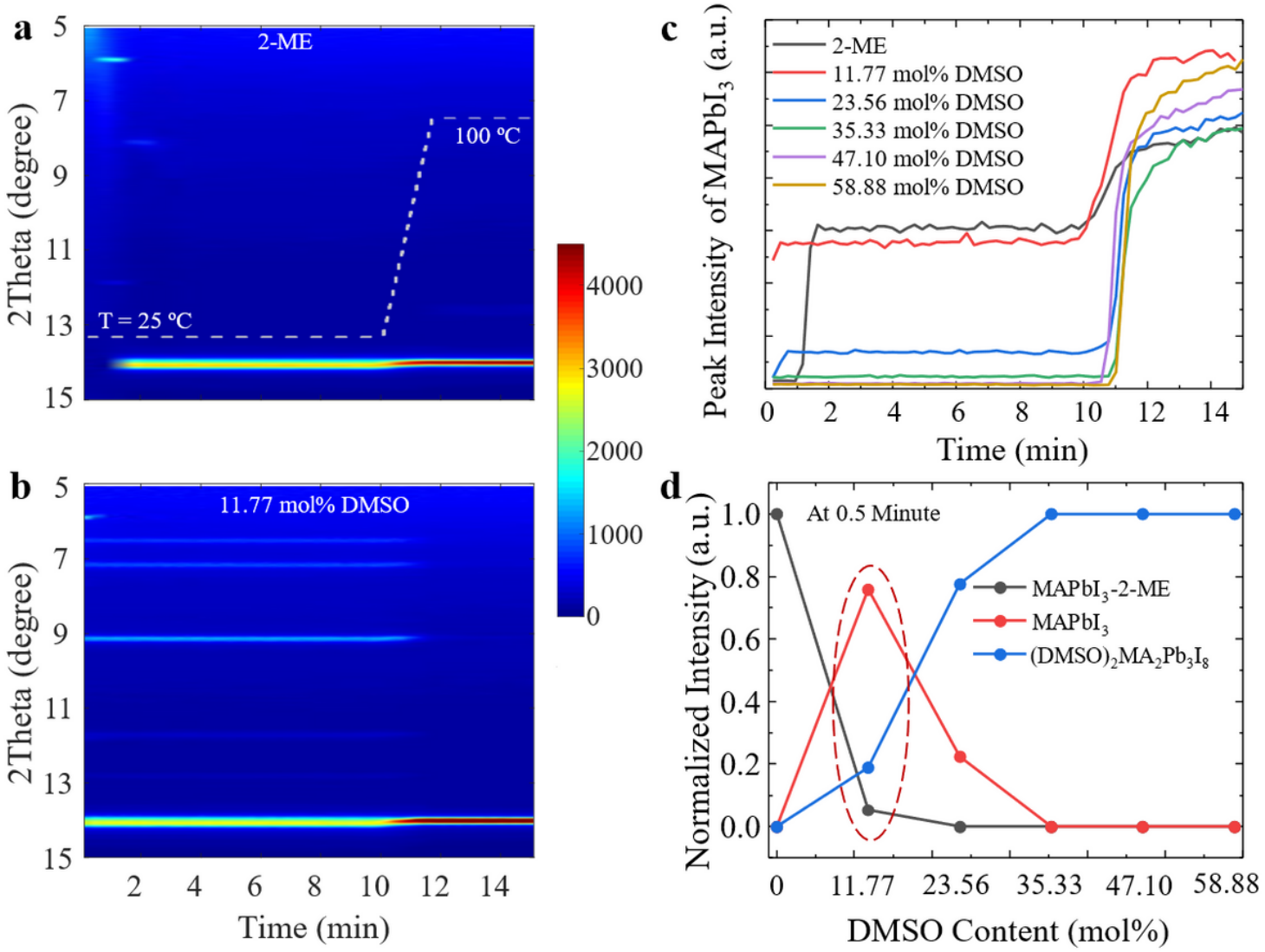

Figure 2

In-situ GIWAXS measurements. a, b Two-dimensional (2D) plots of time resolved in-situ grazing incidence wide-angle X-ray scattering (GIWAXS) of a, 2-ME ink and b, 11.77 mol% 2-ME-DMSO ink (Temperature keep at 25 °C from 0 to 10 min, then accelerating to 100 °C with ramping of 45 °C/min, These experiments were performed at KMC-2 beamline at HZB21). c, normalized peak intensity of MAPbI3 versus of time and d, MAPbI3-2-ME, MAPbI3 and (DMSO)2MA2Pb3I8 as function of DMSO content at 0.5 minute of in-situ GIWAXS pattern.

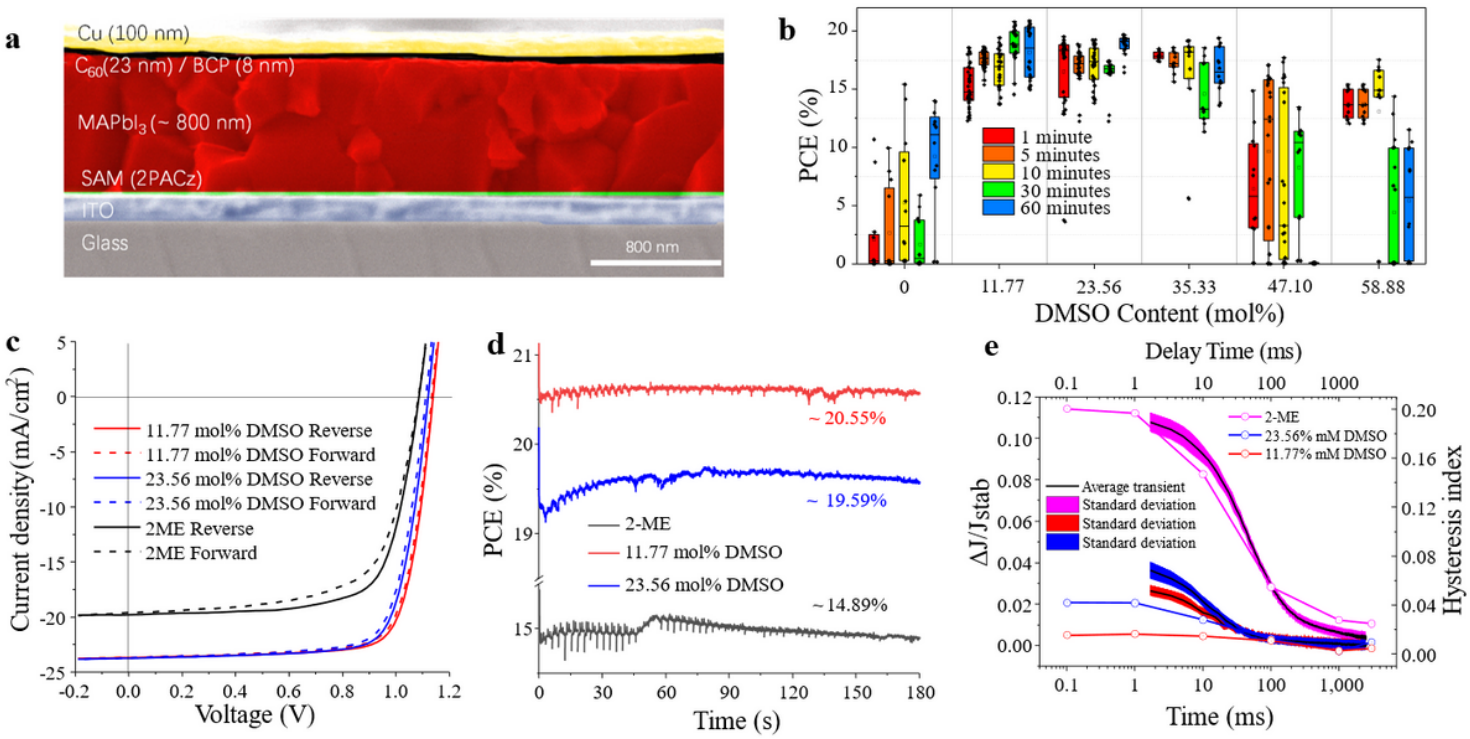

Figure 3

Devices performance and parameters. a, configuration and cross-section images of device made from 11.77 mol% 2-ME-DMSO ink. b, The performance distribution of more than 60 solar cell devices made by 2-ME and 2-ME-DMSO inks was summarized versus storage time. c, the current density–voltage (J–V) scanning (active area is 0.16 cm-2) and d, the stabilized output of the of corresponding devices. e, the differential transient response of devices upon voltage perturbation at MPP (TrAMPPT- cite Anielas paper) ΔJ/Jstab, and hysteresis index (HI) derived from reverse and forward the J-V measurements at different delay times of devices fabricated from 2-ME reference and 11.77 mol% as well as 23.56 mol% DMSO containing 2-ME inks.

Supplementary Files

This is a list of supplementary files associated with this preprint. Click to download.

- SI.docx